Science of the Total Environment 625 (2018) 1518–1526

Contents lists available at ScienceDirect

Science of the Total Environment

journal homepage: www.elsevier.com/locate/scitotenv

Potential impact of natural organic ligands on the colloidal stability of silver nanoparticles

Kamelia Afshinnia, Brandon Marrone, Mohammed Baalousha *

Center for Environmental Nanoscience and Risk, Department of Environmental Health Sciences, Arnold School of Public Health, University South Carolina, Columbia, SC 29208, United States

HIGHLIGHTS

- L-Cysteine and *N*-acetyl L-cysteine decrease cit-AgNP dissolution.
- L-Cysteine destabilizes, whereas *N*-acetyl L-cysteine enhances the stability of cit-AgNPs.
- L-Cysteine reduces the stabilizing effect of Suwannee River fulvic acid.
- Functional groups play a major role in determining the organic ligand on cit-AgNP stability.
- Different NOMs stabilizes cit-AgNPs to different extents.

GRAPHICAL ABSTRACT

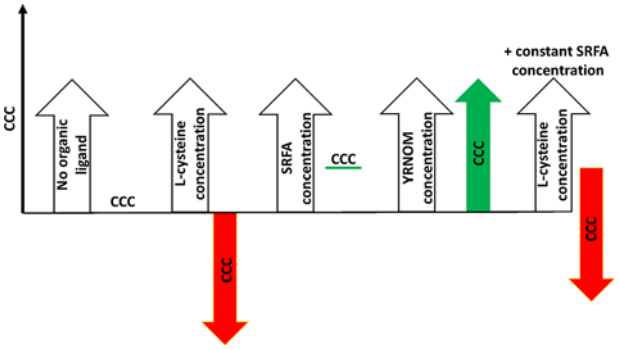

ARTICLE INFO

Article history:
Received 13 October 2017
Received in revised form 24 December 2017
Accepted 25 December 2017
Available online xxxx

Editor: D. Barcelo

Keywords:
Natural organic ligands
Functional groups
Aggregation
Dissolution
Silver nanoparticles

ABSTRACT

Interaction of natural organic matter (NOM) with engineered nanoparticles (NPs) determine NP fate, transport, and environmental persistence. However, the effect of NOM chemical composition, structure, and concentration on aggregation kinetics and dissolution behavior of silver nanoparticles (AgNPs) are still poorly understood because of heterogeneity and variability in NOM and AgNP properties. Here, aggregation behavior of citrate-coated silver nanoparticles (cit-AgNPs with a z-average diameter of 18 nm) was investigated in the presence of L-cysteine (L-cys) and *N*-acetyl L-cysteine (NAL-cys) using UV–vis spectroscopy. We also investigated the effect of Suwannee River fulvic acid (SRFA) and a NOM isolated from the Yukon River (YRNOM) on the stability of cit-AgNPs. The dissolution of cit-AgNPs decreased with increased L-cys and NAL-cys concentration from 0 to 10 μM. The critical coagulation concentration (CCC) of cit-AgNPs decreased in the presence of L-cys and increased in the presence of NAL-cys. Similarly, L-cys destabilizes cit-AgNPs in the presence of SRFA. The differences in the stability of cit-AgNPs in the presence of L-cys and NAL-cys can be attributed to the differences in the functional groups in these two cysteine molecules. L-cys has both negatively charged carboxylic group and a positively charged amine group, resulting in bridging between different particles. NAL-cys is a derivative of cysteine wherein an acetyl group is attached to the nitrogen atom thus shielding the positive charge on the amine group and therefore eliminating the bridging interaction mechanism. SRFA and YRNOM enhanced the stability of cit-AgNPs and increased the CCC value to higher counter ion concentrations. The concentration of SRFA (1–5 mg L^{-1}) did not affect the CCC, whereas the increased concentration of YRNOM increased the CCC of cit-AgNPs to high Na^{+} concentrations likely due to increased sorption of higher molecular weight

* Corresponding author.
E-mail address: mbaalous@mailbox.sc.edu (M. Baalousha).

https://doi.org/10.1016/j.scitotenv.2017.12.299

compounds on the surface of cit-AgNPs. The outcome of this study suggests the importance of understanding the molecular properties of NOM (*e.g.* functional groups and molecular weight) in determining cit-AgNP environmental behaviors.

1. Introduction

The wide use of silver nanoparticles (AgNPs) in consumer products has recently been a focus of concern due to the potential risk from their release to the environment (Fabrega et al., 2011; Gondikas et al., 2012; Levard et al., 2012; Loza et al., 2014; Luoma et al., 2016). Once in the environment, AgNPs undergo several transformations such as surface coating modifications by organic ligands, aggregation, dissolution and sulfidation (Baalousha, 2017; Gondikas et al., 2012; Hotze et al., 2010; Luoma et al., 2016; Peijnenburg et al., 2015). These transformations will impact NP transport, environmental persistence, reactivity, bioavailability and toxicity to exposed organisms (Hotze et al., 2010; Luoma et al., 2016; Peijnenburg et al., 2015). NP transformation processes depend on NP physicochemical properties (*e.g.* size, shape, surface charge, and concentration) and the characteristics of the media (*e.g.* pH, ionic strength, and presence of natural organic macromolecules) (Afshinnia et al., 2017; Hotze et al., 2010; Levard et al., 2012).

NOM is ubiquitous in natural environments and varies in concentration from 0.1 to 10s of mg L^{-1}, depending on biogeochemical and climatic conditions (Filella, 2007; Nebbioso and Piccolo, 2013; Philippe and Schaumann, 2014). NOM is composed of a complex mixture of polyelectrolytic and polyfunctional organic molecules that vary both spatially and temporally in terms of molecular composition, acidity, molecular weight, structure, and charge density (Gu et al., 1995). The main components of NOM are humic substances, polysaccharides, lipids, proteins and other classes of organic molecules (Nebbioso and Piccolo, 2013; Philippe and Schaumann, 2014). The widely diverse composition and properties of NOM (*e.g.* N- and S-content, functional groups, molecular weight, hydrophobicity, *etc.*) will significantly impact the molecular composition of NP surface coating, thereby influencing NP fate, behavior, bioavailability and toxicity (Louie et al., 2015; Luo et al., 2016; Mirshahghassemi et al., 2016; Mirshahghassemi and Lead, 2015; Philippe and Schaumann, 2014; Yi et al., 2016).

In waters and sediments, thiols rich organic ligands are commonly present as a component of the natural organic matter (NOM) in nanomolar to micromolar concentrations (Gondikas et al., 2012). Additionally, thiol-containing biomolecules such as L-cysteine (L-cys) and *N*-acetyl L-cysteine (NAL-cys) are ubiquitously present in biological media such as tissues, blood and bacterial plasma (Gondikas et al., 2012; Luoma et al., 2016; Poblete et al., 2016). The hydrosulfide group in cysteine can form covalent bonds with AgNPs surface and replace the engineered surface coating such as citrate and polyvinyl pyrrolidone (PVP) (Afshinnia et al., 2016; Mandal et al., 2001; Priester et al., 2014; Stewart et al., 2012; Yang et al., 2014a). Cystine, the disulfide form of cysteine, can also modify the surface properties, replace the surface coating and decrease the stability of citrate-coated AgNPs (Afshinnia et al., 2016). Additionally, cysteine has been widely used in AgNP toxicity studies to chelate the released Ag ions from AgNPs and thus to differentiate AgNP toxicity from that of Ag ions assuming that cysteine does not interact or impact the AgNP stability (Foldbjerg et al., 2011; Kawata et al., 2009; Miao et al., 2009).

A survey of literature shows variable effects of cysteine and NOM on AgNPs stability and dissolution dynamics. Whereas Pokhrel et al. (2013) suggested that citrate coated silver nanoparticles (cit-AgNPs) are fairly stable in the presence of cysteine, Yi et al. (2016) demonstrated that cysteine can change the zeta potential and average diameter of AgNPs which may influence the stability of AgNPs in water. Similarly contradictory results has been reported on the effect of NOM on AgNPs stability. Where one study reported that 10 mg L^{-1} of fulvic acid did not have a noticeable effect on AgNP aggregation kinetics (Gunsolus et al., 2015; Li et al., 2010), another study reported an increase in stability (*e.g.*, CCC) in the presence of fulvic acid (Afshinnia and Baalousha, 2017; Baalousha et al., 2013). These apparently contradictory results could be due to the heterogeneity of NOM and AgNPs properties (Baalousha, 2017; Gondikas et al., 2010).

Numerous studies have addressed the effect of inorganic ligands on AgNP dissolution and aggregation (Badawy et al., 2010; Levard et al., 2012, 2013a). However, very little is known on the impact of organic ligands on AgNP dissolution and aggregation. Therefore, the aim of this study is to assess the effect of two thiol containing organic ligands, L-cys and NAL-cys, and two NOM samples (*e.g.* Suwannee River fulvic acid; SRFA and Yukon River NOM; YRNOM) on the colloidal stability and dissolution behavior of cit-AgNPs (500 μg L^{-1}). These two ligands (*e.g.* L-cys and NAL-cys) are selected because of their biological importance; (Guo et al., 2013; Ravindran et al., 2013; Samadi-Maybodi and Akhoondi, 2015) they have been widely used in AgNPs toxicity studies to differentiate between the toxicity of AgNPs and Ag ions (Li et al., 2015); they possess the same number of N- and S-atoms per molecule, yet they have different ionizable functional groups; and they are simple model compounds that will facilitate our understanding of their role in determining AgNP environmental and biological behaviors. SRFA was used as a NOM surrogate and because it has been widely used in the literature (Afshinnia and Baalousha, 2017; Afshinnia et al., 2016). Yukon River NOM was used as an example of a more complex NOM compared to SRFA as it was isolated by ultrafiltration and likely to include a wider variety of NOM molecules and therefore likely to have a different impact on AgNP environmental behaviors.

2. Methodology

2.1. Synthesis and characterization of AgNPs

Citrate-coated silver nanoparticles (cit-AgNPs) were synthesized using a previously reported method (Afshinnia and Baalousha, 2017; Mitra et al., 2017; Romer et al., 2011). Briefly, solutions of 0.25 mM silver nitrate (99.9 +%, Alfa Aesar), 0.31 mM trisodium citrate (99.9 +%, British Drug Houses, BDH) and 10 mM sodium borohydride (98%-Alfa Aesar) were prepared in ultrahigh purity water (UHPW, resistivity = 18.2 MΩ·cm) and were kept at 4 °C in the refrigerator for 30 min. Silver nitrate and sodium citrate solutions were mixed together in a conical flask under continuous stirring condition. Then, 6 mL of the reducing agent, sodium borohydride (NaBH4), was added into the batch. After 10 min of stirring, the solution was heated to 100 °C for a further 90 min. The synthesized AgNPs was stored overnight in dark at room temperature and then cooled to 4 °C. Afterwards, 200 mL AgNP suspension was cleaned using a pressurized stirred ultrafiltration cell (Amicon, 3 kDa regenerated cellulose membrane, Millipore) to remove the excess reagents before use. During the washing process, AgNP suspension volume was reduced to 100 mL and then replenished by 100 mL of 0.31 mM trisodium citrate solution. This process was repeated four times.

The concentration of the synthesized cit-AgNPs was measured by inductively coupled plasma-atomic emission spectroscopy (ICP-OES; Varian 710-ES). The total Ag concentration of the stock suspension was 9.37 ± 0.23 mg L^{-1}. The size and electrophoretic mobility (EPM) of cit-AgNPs were determined by dynamic light scattering (DLS) and laser Doppler electrophoresis, respectively using a Malvern Zetasizer NanoZS Instrument (Malvern, USA). The

Malvern Zeta potential transfer standard (DTS 1235) consisting of a polystyrene latex in aqueous buffer at pH 9 with a zeta potential value of −42 ± 4.2 mV was used to verify the performance of the instrument and zeta potential cell throughout the experiments. The z-average hydrodynamic diameter and size polydispersity index of synthesized cit-AgNPs in stock suspension were 18.24 ± 0.22 nm and 0.22 ± 0.01, respectively. The zeta potential of the synthesized cit-AgNPs (pH 7.0) was −41.7 ± 2.0. Here, the standard deviation value represents the reliability of the replicate measurements and was determined from 5 replicates of size and 10 replicates of zeta potential. The number average core size measured by transmission electron microscopy (TEM) is approximately 10 nm (Baalousha and Lead, 2013). The smaller core size measured by TEM is attributed to particle dispersity and average weighing; that is number weighing for core size measured by TEM *vs.* intensity weighing for z-average hydrodynamic diameter measured by DLS (Baalousha and Lead, 2012).

2.2. Cit-AgNP behavior by UV–vis spectroscopy

The behavior (aggregation, dissolution, and sedimentation) of cit-AgNPs suspended in different concentrations of L-cys and NAL-cys was monitored over 72 h using a UV–vis spectrophotometer (UV-2600 Shimadzu, Santa Clara, CA, USA). All suspensions were buffered at pH 7.0 using 0.1 mM potassium phosphate monobasic. The low K^+ concentration from the buffer is unlikely to have any effect on cit-AgNP stability compared to Na^+ due to the higher affinity of Na^+ than K^+ to the carboxylate groups (Pokhrel et al., 2014). Aliquots of cit-AgNP suspension, and L-cys, NAL-cys, and phosphate buffer stock solutions were mixed together in a total volume of 120 mL prior to analysis by UV–vis to achieve final concentrations of 500 μg L^{-1} AgNPs, 0.1 mM phosphate buffer, and different concentrations of L-cys and NAL-cys (0.01–10 μM). Cit-AgNP concentration of 500 μg L^{-1} Ag was used in this study to enable measurement of AgNP absorption and absorbance spectra by UV–vis. Aliquots of AgNPs-L-cys and AgNPs-NAL-cys mixtures were extracted at different time points for UV–vis analysis, and pH measurement, which varied within a narrow range *e.g.*, 6.6 to 6.8 among the different sampling times.

UV–vis spectra can provide a lot of information on NP behavior including their aggregation, dissolution and sedimentation. However, results can be convoluted and difficult to interpret if all processes occur at the same time. Decrease in UV–vis absorbance at λ_{max} indicates particle aggregation and/or dissolution (Baalousha et al., 2013, 2015). In the absence of aggregation, dissolution can be assumed to be responsible for the decrease in UV–vis absorbance at λ_{max} (Baalousha et al., 2013, 2015). Aggregation results in the formation of a second peak at higher wavelength centered on approximately λ_{max} (indicated here as $\lambda_{agg\ max}$) of 500–600 nm which increases initially with the increase in NP aggregation and then decreases with NP aggregate sedimentation. This decrease in $\lambda_{agg\ max}$ was used as indication of AgNP aggregate sedimentation.

In order to further underpin UV–vis analysis, the dissolved Ag fraction was separated by centrifugal ultrafiltration using Amicon Ultra-4 filtration cartridges at 3 kDa membrane (Millipore). Samples were centrifuged at 4000*g* for 20 min using an Eppendorf 5810R Centrifuge and the dissolved Ag concentration in the filtrate was measured by ICP-OES.

2.3. Aggregation kinetics

Two NOM samples were used in the aggregation kinetic experiment including SRFA (International Humic Substances Society, USA) and dissolved NOM (1 kDa-0.45 μm) isolated from the Yukon River, Alaska, USA using ultrafiltration method (Guo and Macdonald, 2006). Stock suspensions of SRFA and YRNOM were prepared by dissolving 2 mg of the NOMs in 10 mL ultrahigh purity water. The NOM suspension pH was adjusted to 7.0 by adding an appropriate amount of 0.1 or 1 M NaOH. The NOM suspensions were then filtered using a 100 nm syringe filter (Hydrophilic Polyvinylidene Fluoride, Millipore) to remove any aggregated molecules.

A stock solution of 1 M sodium nitrate was freshly prepared to make different concentrations of the monovalent electrolyte. Aliquots of AgNPs and SRFA or AgNPs and YRNOM stock suspension were mixed together to obtain mixtures with final concentrations of 500 μg L^{-1} AgNPs and 1 mg L^{-1} NOM. The mixtures were then left for 3 h in the fridge at 4 °C to reach equilibrium before performing the aggregation kinetics' experiment. Similar to the experiment with NOM, stock solutions of 0.1 mM L-cys and NAL-cys were prepared. In order to prepare different concentrations of L-cys and NAL-cys, aliquots of the cysteine solutions were mixed with AgNPs for 3 h prior to the aggregation kinetics' experiment. For aggregation kinetics analysis, aliquots of each of the prepared NOM-AgNPs mixtures were added to a mixture of different volumes of buffered sodium nitrate solution and buffered UHPW.

AgNP aggregation kinetics was performed by UV–vis according to the method described elsewhere (Baalousha et al., 2013). The aggregation rate constant (k) during the initial stage of the aggregation is proportional to the rate of the loss in the UV–vis absorbance at the specific Plasmon resonance peak of primary AgNPs (λ = 394 nm) (Moskovits and Vlckova, 2005). The slope of the loss in the UV–vis absorbance at λ = 394 nm within the first 30 s of mixing AgNPs with sodium nitrate was fitted by linear correlation function. The 30 s time to measure NPs aggregation kinetics ensures that the reduction in the UV–vis absorbance is only due to AgNP aggregation (Afshinnia et al., 2016; Baalousha et al., 2013). The attachment efficiency (α) *versus* sodium nitrate concentration, which is used to characterize NP stability is calculated according to Eq. (1) (Li et al., 2012).

$$\alpha = \frac{K_{Slow}}{K_{Fast}} \quad (1)$$

Where K_{slow} and K_{fast} represent the aggregation rate constants under reaction (RLA) and diffusion (DLA) limited aggregation regimes. K_{fast} is the average of all aggregation rate constants measured under DLA regime using the same experimental conditions of NP and buffer concentrations. The RLA regime occurs when electrolyte concentration is below the CCC, where NP interaction is driven by electrostatic energy barrier resulting from electrostatic double layer repulsion forces and van der Waals attractions forces. DLA occurs at electrolyte concentration higher than the CCC, where excess electrolyte ions completely screen the surface energy barriers and aggregation process is only driven by NP diffusion (Afshinnia et al., 2016; Li et al., 2012). The CCC is the minimum concentration of sodium nitrate required to completely screen the NP surface charge. The attachment efficiencies under RLA and DLA regimes were plotted as a function of electrolyte concentration for different concentrations of L-cys, NAL-cys, SRFA and YRNOM, and the mixture of L-cys and SRFA. Attachment efficiencies under slow and fast aggregation regimes were fitted by linear functions and their intersection yields the CCC (El Badawy et al., 2012). All measurements were repeated 3 times and the means and standard deviations of 3 replicates of attachment efficiencies are presented in the relevant figures.

3. Results and discussion

3.1. Effect of L-cys and NAL-cys on cit-AgNP aggregation and dissolution behavior

Fig. 1 shows the dissolution of cit-AgNPs (500 μg L^{-1}) following the interaction with L-cys and NAL-cys in the presence of 0.1 mM phosphate buffer. The concentration of dissolved Ag increases from *ca.* 70 to 145 μg L^{-1} in the absence of L-cys and NAL-cys over 72 h. However, both L-cys and NAL-cys reduce the dissolution of AgNPs compared to that in the absence of L-cys and Nal-Cys, and the reduction in AgNP dissolution increases with increased cysteine concentrations. At 0.1 μM L-cys

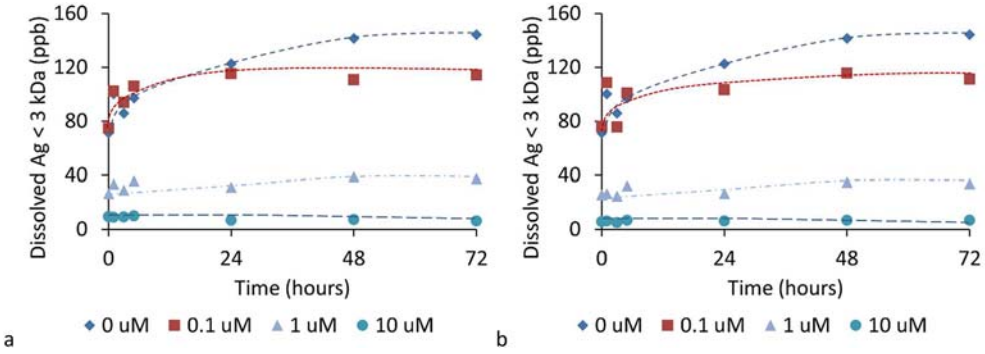

Fig. 1. Dissolution of cit-AgNPs (500 μg L^{-1}) following the interaction with different concentrations of (a) L-cys, and (b) NAL-cys. All suspensions were buffered with 0.1 mM potassium phosphate monobasic buffer. Dashed lines are used to guide the readers' eyes.

(Fig. 1a) or NAL-cys (Fig. 1b), dissolved Ag concentrations increases from 75 to 110 μg L^{-1}, indicating slightly decreased dissolution compared to the absence of L-cys, or NAL-cys. At higher (≥ 1 mM) L-cys and NAL-cys concentrations, dissolved Ag concentration decreased immediately from 70 μg L^{-1} in the absence of L-cys or NAL-cys to 35 and 5 μg L^{-1} in the presence of 1 and 10 μM L-cys and NAL-cys concentrations respectively, indicating a significant decrease in AgNP dissolution. Both L-cys and NAL-cys possess thiol group which interact with silver *via* a strong covalent (thiolate) bond with a stability constant of 10^{13} (Adams and Kramer, 1999; Yang et al., 2014b). Therefore, L-cys and NAL-cys adsorb onto the NP surface with its thiol group, resulting in the formation of Ag_2S layer on the surface of AgNPs and thus inhibit the dissolution by preventing the subsequent oxidation of AgNPs (Loza et al., 2014; Priester et al., 2014). The reduced dissolution of AgNPs by cysteine has been reported in previous studies (Liu et al., 2011; Loza et al., 2014; Yi et al., 2016). For example Sigg et al. reported a decrease in dissolved Ag concentrations in the presence of 0.5 to 5 μM cysteine over 24 h compared to the absence of L-cys (Sigg and Lindauer, 2015). However, our results contradict the previous study by Gondikas et al. in which they observed the increase in dissolved Ag concentration released from cit-AgNPs in the presence of L-cys (Gondikas et al., 2012). These apparently contradictory results could be due to the different experimental conditions such as L-cys and total Ag concentration (Gondikas et al., 2012). The higher cys/Ag ratio (400 μM cysteine/8 μM AgNPs) used in Gondikas et al. could result in the occurrence of high number of free cysteine molecules in the solution which may act as a sink for dissolved Ag and accelerate their dissolution in a similar manner to the effect of chloride on AgNP dissolution. At low Cl/Ag concentration, Cl tends to reduced AgNP dissolution, whereas at high Cl/Ag concentration, Cl tend to increases AgNP dissolution (Baalousha et al., 2016; Levard et al., 2013b).

The UV–vis spectra of cit-AgNPs after mixing with different concentrations of L-cys and NAL-cys in the presence of 0.1 mM phosphate buffer are presented in Fig. 2a-h. In the absence of cysteine, the primary AgNPs have a maximum absorbance ($\lambda_{prim\ max}$) centered at 394 nm. At the very low concentration of L-cys, 0.01 μM (Fig. 2a), the UV–vis absorbance at 394 nm decreased to lower values over the 72 h period without peak broadening or formation of a second UV–vis absorbance peak at higher wavelengths, indicating the loss of primary cit-AgNPs in the presence of L-cys most likely by dissolution. At 0.1 μM L-cys (Fig. 2c), a loss in the UV–vis absorbance at 394 nm is observed accompanied by the appearance of a second UV–vis absorbance peak toward higher wavelengths. This second peak is indicative of NP aggregate formation and is centered on $\lambda_{agg\ max} = 560$ nm. At 1 μM M L-cys concentration (Fig. 2e), a similar decrease in the primary NP UV–vis absorbance was observed as for the 0.1 μM M L-cys concentration, however, the maximum aggregate UV–vis absorbance was centered on shorter wavelength (*ca.* $\lambda_{agg\ max} = 500$ nm), which may attributed to the rapid sedimentation of larger AgNP aggregates as $\lambda_{agg\ max}$ is directly proportional to aggregate size (Paramelle et al., 2014). This sedimentation behavior is more apparent at the highest L-cys concentration (*e.g.* 10 mM L-cys, Fig. 2g), where the UV–vis spectrum indicates the formation of a shoulder at around 450 to 550 nm immediately after interaction with L-cys, which remained apparent with a decreased intensity up to 5 h. After 24 h, the UV–vis absorbance shifted to smaller wavelength and the primary particle absorbance was centered on *ca.* $\lambda_{prim\ max}$ of 350–360 nm indicating that only small AgNPs remain in suspension. Sedimentation results in the removal of large AgNP aggregates, leaving behind the smallest AgNPs that remain in suspension and results in absorbance peak around *ca.* 350–360 nm (Moosa et al., 2015). The selective aggregation and sedimentation of larger particles can be attributed to the size-dependent stability of AgNPs. For instance, Afshinnia et al. demonstrated that larger NPs have smaller CCC values compared with smaller NPs (Afshinnia et al., 2017). Frens (1972) demonstrated that NPs with smaller sizes are more stable against electrolyte coagulation than coarser suspensions (Frens, 1972). He used this observation to separate larger NPs from a mixture of small and large NPs by selective aggregation of large particles.

UV–vis spectra in the presence of NAL-cys are presented in Fig. 2b, d, f, and h. Result shows a slight broadening of the UV–vis absorbance peak centered at 394 nm with the increase in NAL-cys concentration from 0.01 to 10 μM suggesting limited aggregation (formation of few doublets and triplets) of AgNPs. The absence of a second peak at higher wavelengths indicates that AgNP aggregation is less extensive in the presence of NAL-cys compared to the aggregation in the presence of L-cys. The differences in AgNP aggregation behavior in L-cys and NAL-cys solutions is attributed to the difference in the structure of these two organic molecules. L-cys possesses both carboxylic and amine groups. NAL-cys is a derivative of L-cys where an acetyl group is attached to the nitrogen atom. Therefore, at/near neutral pH values, L-cys forms a dipolar ion "zwitterion", where the carboxylic group is negatively charged and the amine group is positively charged. The negative charge on the surface of one particle interacts with the positive charge on the surface of another particle inducing AgNP aggregation through bridging mechanism (Brewer et al., 2005; Horovitz et al., 2007; Ravindran et al., 2013). On the other hand, at/near neutral pH, NAL-cys possesses only one negative charge, thus resulting in a reduction of cit-AgNPs surface charge, which explains the slight aggregation indicated by the broadening of the UV–vis absorbance of primary AgNPs. The shielding of the positive charge of the amine group by the acetyl group prevents AgNP aggregation by preventing bridging mechanism. Additionally, NAL-cys has a higher molecular weight (163.19 g mol^{-1}) compared with L-cys (121.16 g mol^{-1}) due to the addition of the acetyl group, which may provide some additional steric stability to AgNPs. Louie et al. (2013) demonstrated that higher molecular weight ligands (NOM) increase NP stability (Louie et al., 2013).

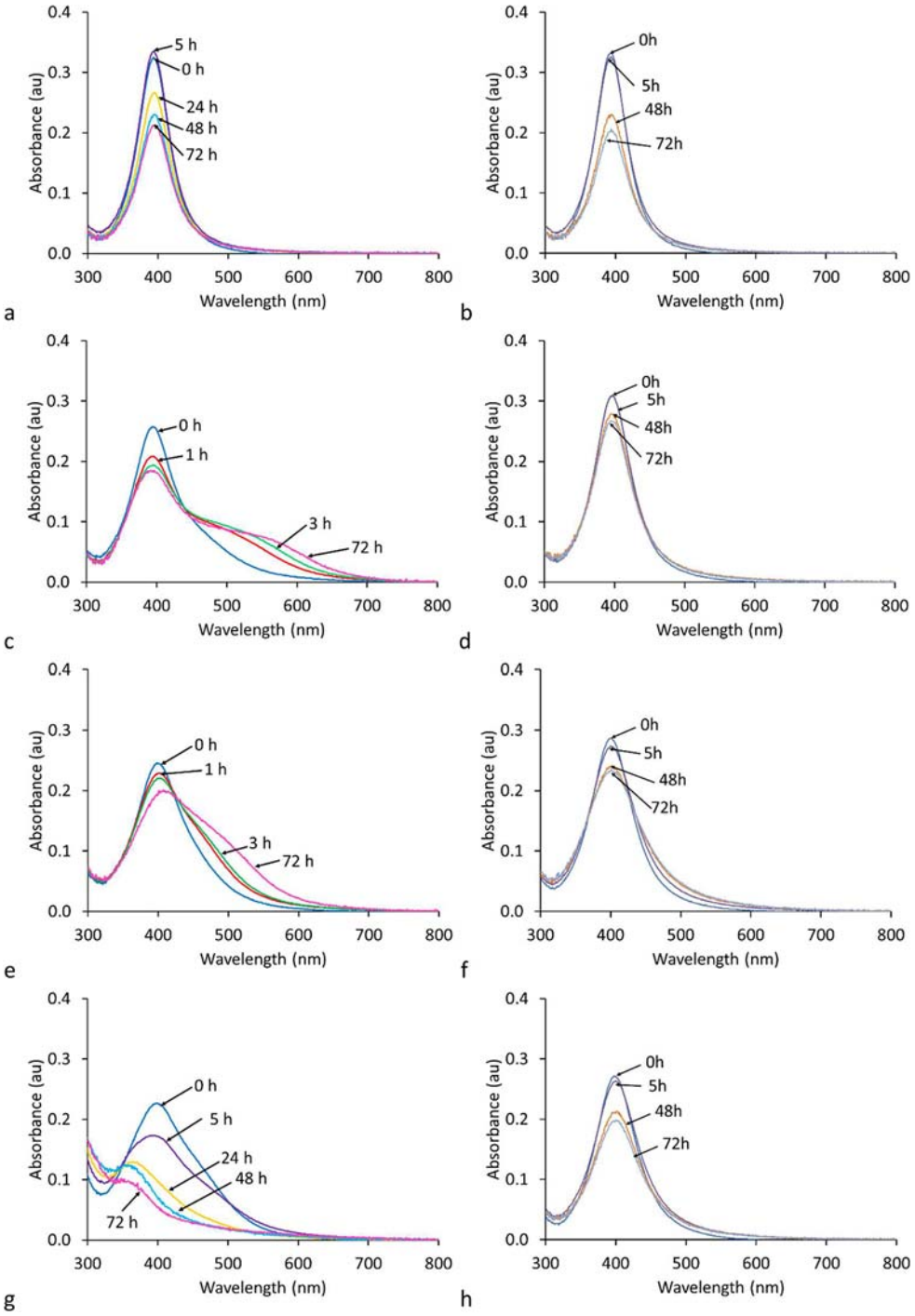

Fig. 2. UV-vis absorbance of cit-AgNPs (500 μg L^{-1}) following interaction with different concentrations of L-cys (a, c, e, and g) and NAL-cys (b, d, f, and h): (a, b) 0.01 μM, (c, d) 0.1 μM, (e, f) 1 μM, and (g, h) 10 μM. All suspensions were buffered with 0.1 mM potassium phosphate monobasic buffer.

3.2. Effect of L-cys and NAL-cys on cit-AgNP aggregation kinetics

The impact of cysteine ligands on the stability of cit-AgNPs in the presence of electrolyte ($NaNO_3$) was assessed by studying the aggregation kinetics of cit-AgNPs in the presence of different concentrations of L-cys and NAL-cys (Figs. 3 and 4). In order to measure the aggregation kinetics' parameters (*e.g.* α and CCC), the loss of UV–vis absorbance of primary NPs due to the aggregation in the presence of $NaNO_3$ at 0.01 and 0.1 μM L-cys (Fig. 3a) and 0.01 μM NAL-cys (Fig. 3b) was monitored at $\lambda = 394$ nm over 10 min and the slope of the loss in UV–vis absorbance was calculated over the first 30 s as described above. The rate of UV–vis absorbance loss at $\lambda = 394$ nm increased with the increase in $NaNO_3$ concentration. In general, lower electrolyte concentrations (*ca.* 50–225 mM $NaNO_3$, Fig. 3a) were required to induce aggregation of cit-AgNPs in the presence of L-cys compared to NAL-cys (*ca.* 100–350 $NaNO_3$, Fig. 3b). In other words, $NaNO_3$ is more efficient in aggregating cit-AgNPs in the presence of L-cys compared to NAL-cys.

The attachment efficiencies of cit-AgNPs as a function of $NaNO_3$ concentration in the presence of L-cys and NAL-cys are presented in Fig. 4. With the increase in L-cys concentration, the attachment efficiency profile shifts toward lower electrolyte concentrations. In other words, at the same electrolyte concentration, the attachment efficiency increases

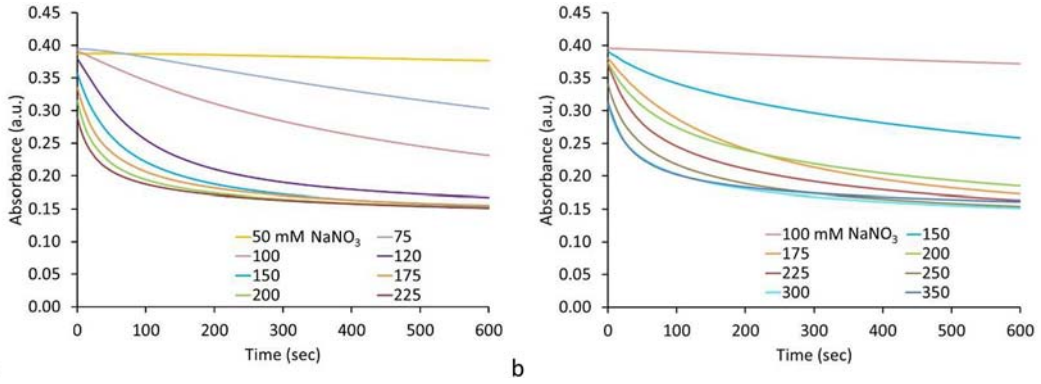

Fig. 3. Evolution of the UV–vis absorbance at λ_{394} of cit-AgNPs (500 μg L^{-1}) as a function of time immediately after mixing with different concentrations of $NaNO_3$ at 0.1 mM phosphate buffer (pH 7.0): (a) 0.01 μM L-cys, and (b) 0.01 μM NAL-cys.

and thus the stability of AgNPs decreases with the increase L-cys concentration. In the presence of NAL-cys, the attachment efficiency profile shifts toward higher electrolyte concentrations. In other words, at the same electrolyte concentration, the attachment efficiency decreases and thus the stability of AgNPs increases in the presence of NAL-cys. The CCC values calculated based on the attachment efficiency profiles are reported in Table 1. Cit-AgNPs have a CCC value of 186.4 ± 7.6 mM Na^+ in the presence of 0.1 mM buffer. The CCC value decreased to 157.0 ± 17.1 and 14.7 ± 2.4 mM Na^+ in the presence of 0.01 and 0.1 μM L-cys, respectively, in good agreement with previous studies reporting decreased stability of AgNPs in the presence of L-cys (Gondikas et al., 2012; Yang et al., 2014a; Yi et al., 2016). Conversely, the CCC increased to 246.0 ± 22.4 mM Na^+ in the presence of 0.01 μM NAL-cys. The decrease in CCC with the increase in L-cys concentration can be due to the higher abundance of L-cys molecules per AgNP surface, resulting in an increased number of L-cys per unit surface area of AgNPs, thus increased number of positively and negatively charged functional groups that can attract each other and reduce the stability of AgNPs. The increased stability of cit-AgNPs following interaction with NAL-cys is because NAL-cysteine replaces citrate coating on the surface of AgNPs, and most likely induces steric stabilization due to its higher molecular weight compared to L-cys, in addition to electrostatic stabilization due to the carboxylic group.

3.2.1. Effect of SRFA and L-cys on cit-AgNP aggregation kinetics

In the natural environment, cysteine molecules (or thiol containing organic ligands) occur as part NOM; that is a complex mixture of thousands of organic molecules. Thus, this section investigates the effect of a mixture of cysteine molecules with SRFA on the stability of cit-AgNPs in order to illustrate the impact of the structure (*e.g.* functional groups) of thiol containing molecules (L-cys) on the stability of AgNPs. The attachment efficiencies of cit-AgNPs in the presence of SRFA and at different L-cys concentrations are presented in Fig. 5. In the presence of SRFA alone, the attachment efficiency profile shifts to higher electrolyte concentrations indicating increased stability of AgNPs. In the presence of SRFA and L-cys, the attachment efficiency profile shift to lower electrolyte concentrations, with an increased shift at higher L-cys concentration, compared with that in the presence of SRFA alone indicating decreased stability in the presence of L-cys. The CCC shifted to higher counter ion concentration (245.7 ± 5.8 mM Na^+) in the presence of 1 mg L^{-1} SRFA compared to the CCC in the absence of SRFA (186.4 mM Na^+, Table 1). This is in agreement with the consensus that SRFA sorbs on the surface of cit-AgNPs *via* ligand exchange mechanism and enhance AgNP stability *via* electrosteric mechanism (Afshinnia and Baalousha, 2017; Afshinnia et al., 2016, 2017; Hotze et al., 2010; Huynh and Chen, 2011; Wijnhoven et al., 2009). The CCC shifted to lower counter ion concentration with the increase in L-cys concentration (217.0 ± 5.6 and 75.6 ± 8.5 mM Na^+ at 0.01 and 0.1 μM, Fig. 5 and Table 1) compared to the CCC in the presence of SRFA (245.7 ± 5.8 mM Na^+).

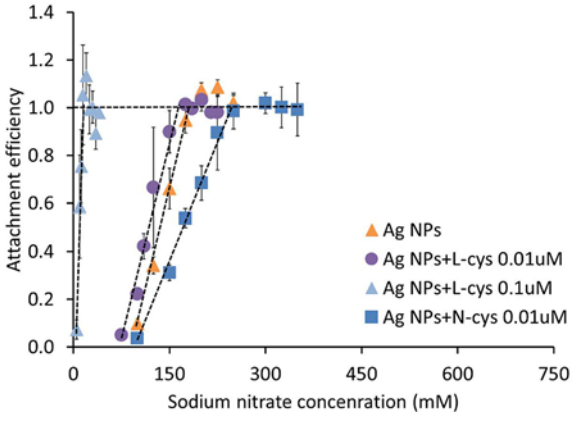

Fig. 4. Attachment efficiency of cit-AgNPs (500 μg L^{-1}) in the presence of L-cys and NAL-cys. Dashed lines are used to guide the readers' eye.

3.2.2. Effect of SRFA and YRNOM on the aggregation kinetics of cit-AgNPs

Attachment efficiencies of AgNPs in the presence of NOM (SRFA and YRNOM) are presented in Fig. 6. At the same $NaNO_3$ concentration, the attachment efficiency is lower in the presence of NOM suggesting that AgNPs have fewer tendencies to aggregate in the presence of NOM. The CCC increases in the presence of SRFA and YRNOM (Fig. 6 and Table 1) due to sorption of NOM molecules on the surface of AgNPs as discussed above (Grillo et al., 2015; Louie et al., 2015; Thio et al., 2011; Zhang et al., 2012). SRFA and YRNOM stabilized AgNPs to the same extent (*e.g.* CCC 245.7 ± 5.8 and 248.0 ± 3.3, respectively) at 1 mg L^{-1} (Fig. 6a and Table 1). The CCC increased slightly to 259.1 mM Na^+ with the increase in SRFA concentration to 5 mg L^{-1} (Fig. 6b and Table 1). However, the CCC increased by approximately two-fold to 512.7 ± 12.7 mM Na^+ with the increase in YRNOM

Table 1
CCC values for cit-AgNPs in the presence of different natural organic matter ligands.

Sample	CCC
AgNPs + L-cys 0.1 μM	14.7 ± 2.4
AgNPs + SRFA + L-cys 0.1 μM	75.6 ± 8.5
AgNPs + L-cys 0.01 μM	157.0 ± 17.1
Ag alone	186.4 ± 7.6
AgNPs + SRFA + L-cys 0.01 μM	217.0 ± 5.6
AgNPs + SRFA 1 mg L^{-1}	245.7 ± 5.8
AgNPs + NAL-cys	246.0 ± 22.4
AgNPs + YRNOM 1 mg L^{-1}	248.0 ± 3.3
AgNPs + SRFA 5 mg L^{-1}	259.1[a]
AgNPs + YRNOM 5 mg L^{-1}	512.7 ± 12.7

[a] Only one replicate was performed here.

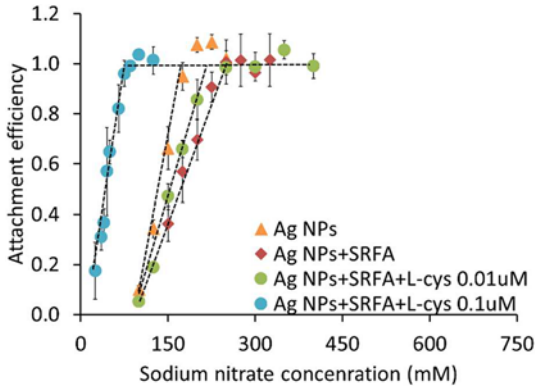

Fig. 5. Attachment efficiency of cit-AgNPs (500 μg L^{-1}) in the presence of L-cys and 1 mg L^{-1} SRFA. Dashed lines are used to guide the readers' eye.

concentration to 5 mg L^{-1} (Fig. 6b and Table 1). We speculate that the differences in the behavior of AgNPs in the presence of SRFA and YRNOM can be attributed to the differences in NOM isolation protocol. Whereas SRFA were isolated by XAD resin and acidification, YRNOM sample was isolated by ultrafiltration at 1 kDa. Thus, YRNOM is more polydisperse compared to SRFA and contains fulvic and humic acids, as well as other fractions of NOM.

Additionally, the increased YRNOM concentration results in an increase in the molecular weight of the YRNOM molecules sorbed on the surface of AgNPs due to the selective sorption of higher molecular weight fractions compared with low molecular weight fractions (Yin et al., 2015). Analysis of the molecular weight of YRNOM formulas that selectively sorbed (*e.g.*, removed from solution following interaction with AgNPs) on the surface of AgNPs by Fourier transform-ion cyclotron-mass spectroscopy suggests that the molecular weight of YRNOM formulas that selectively sorbed on the surface of AgNPs increased from 669 Da to 716.2 Da with the increase in YRNOM concentration from 1 to 5 mg L^{-1} in the presence of 4 mg L^{-1} AgNPs (data not published yet). This is likely to increase the stability of AgNPs, in good agreement with previous studies (Louie et al., 2013). It is worth mentioning here that the NOM molecular weight determined by FT-ICR-MS is <1 kDa, in agreement with previous reports of the supramolecular assembly concept (Piccolo, 2001).

4. Recommendations and future directions

NOM has been reported to increase the stability of engineered nanoparticles, and some studies suggested that nitrogen- and sulfur-rich NOM more significantly increases the stability of AgNPs (Gunsolus et al., 2015). However, the role of N and S atoms in determining NP stability depends on the functional groups containing these atoms. Therefore, understanding the role of molecular formula structure (functional groups) in determining NP stability is essential for predicting the transport and eventual fate of NPs as well as NP bioavailability and toxicity.

In this study, the attachment efficiencies of AgNPs were measured under different conditions that include SRFA, SRFA mixed with L-cys and NAL-cys, and a NOM extracted by ultrafiltration from the Yukon River. Here we illustrate that, not only the elemental composition, but also that the molecular structure (functional groups) of the organic ligands play a significant role in determining the stability of NPs. Whereas NAL-cys increased the stability of AgNPs, L-cys decreased the stability of AgNPs. Additionally, whereas SRFA increased the stability of AgNPs, addition of a mixture of SRFA and L-cys decreased the stability of AgNPs. It is worth noting here that both L-cys and NAL-cys contain the same number of N and S atoms per molecule. However, NAL-cys is a derivative of cysteine wherein an acetyl group is attached to the nitrogen atom, thus neutralizing the positive charge on the amine group in the L-cys molecule. This study illustrates the need for a better and more in-depth characterization of NOM at the molecular level to better understand the role of NOM in determining the environmental behavior and effects of NPs. A combination of analytical bulk and molecular level characterization tools such as NOM, FTIR, and ultrahigh resolution-mass spectroscopy techniques such as Fourier transform-ion cyclotron-mass spectroscopy are likely needed to achieve such in depth understanding of NOM and its role in modulating NP environmental fate and behavior.

Both L-cys and NAL-cys has been used in ecotoxicological studies (Luoma et al., 2016) to scavenge dissolved ions (*e.g.* Ag). However, no study has considered the cysteine-induced AgNP destabilization on AgNP uptake and toxicity. The decreased stability of AgNPs in the presence of L-cys could contribute to the decreased uptake and/or toxicity of AgNPs reported in the literature, which should be further investigated in future studies. Given that both L-cys and NAL-cys equally reduce the dissolution of AgNPs and that NAL-cys increases the stability of AgNPs in electrolyte solution, NAL-cys is recommended as a better alternative in ecotoxicological studies to scavenge dissolved Ag ions.

Additionally, we illustrate that whereas the concentration of SRFA does not significantly impact the stability of AgNPs, the increased concentration of YRNOM increases the stability of AgNPs due to the increased selective sorption of higher molecular weight NOMs on the surface of AgNPs, which increases the steric stabilization of AgNPs. SRFA, extracted by XAD resin, represents a subgroup of NOM characterized by low molecular weight; whereas YRNOM, extracted by ultrafiltration and thus containing a mixture of fulvic and humic acids as well as other NOM molecules are more complex and contain molecular formulas of higher molecular weight, which selectively sorb on the surface of NPs (Louie et al., 2015). Therefore, this study illustrates that the impact of NOM on NP stability may also depend on the extraction protocol. Studying both XAD-extracted fractions together with total NOM fractions "isolated by ultrafiltration" is ideal to better understand the roles of NOM in determining NP environmental and biological interactions. NOM isolates are simpler and therefore are better suited for mechanistic understanding of NOM-NP interactions, whereas total NOM samples are

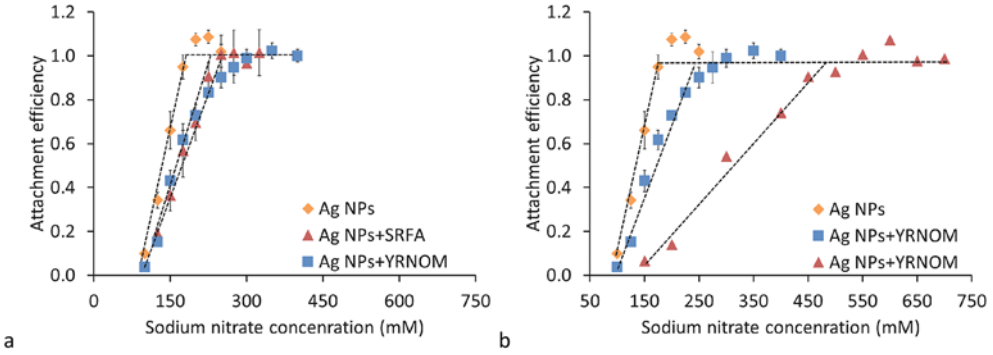

Fig. 6. Attachment efficiency of cit-AgNPs (500 μg L^{-1}) (a) in the presence of 1 mg L^{-1} SRFA and YRNOM, and (b) in the presence of 5 mg L^{-1} SRFA and YRNOM. Dashed lines are used to guide the readers' eye.

more environmentally realistic and will provide better information on the expected environmental behaviors of NPs.

Finally, this work underscores the importance of understanding the impact of NOM molecular properties (*e.g.* molecular composition and structure, molecular weight, *etc.*) on NP stability in both ecotoxicological media as well as in the natural environment, and thus the fate and effects of NPs.

Acknowledgment

We acknowledge funding from the National Science Foundation (NSF1437307). Yukon River natural organic matter was donated by Prof. Laodong Guo at the School of Freshwater Sciences at the University of Wisconsin-Milwaukee.

Appendix A. Supplementary data

Supplementary data to this article can be found online at https://doi.org/10.1016/j.scitotenv.2017.12.299.

References

Adams, N.W.H., Kramer, J.R., 1999. Silver speciation in wastewater effluent, surface waters, and pore waters. Environ. Toxicol. Chem. 18 (12), 2667–2673.
Afshinnia, K., Baalousha, M., 2017. Effect of phosphate buffer on aggregation kinetics of citrate-coated silver nanoparticles induced by monovalent and divalent electrolytes. Sci. Total Environ. 581, 268–276.
Afshinnia, K., Gibson, I., Merrifield, R., Baalousha, M., 2016. The concentration-dependent aggregation of Ag NPs induced by cystine. Sci. Total Environ. 557-558, 395–403.
Afshinnia, K., Sikder, M., Cai, B., Baalousha, M., 2017. Effect of nanomaterial and media physicochemical properties on Ag NM aggregation kinetics. J. Colloid Interface Sci. 487, 192–200.
Baalousha, M., 2017. Effect of nanomaterial and media physicochemical properties on nanomaterial aggregation kinetics. NanoImpact 6, 55–68.
Baalousha, M., Lead, J.R., 2012. Rationalizing nanomaterial sizes measured by atomic force microscopy, flow field-flow fractionation, and dynamic light scattering: sample preperation, polydipsersity, and particle structure. Environ. Sci. Technol. 46 (6134-4142).
Baalousha, M., Lead, J.R., 2013. Nanoparticle dispersity in toxicology. Nat. Nanotechnol. 8, 308–309.
Baalousha, M., Nur, Y., Römer, I., Tejamaya, M., Lead, J.R., 2013. Effect of monovalent and divalent cations, anions and fulvic acid on aggregation of citrate-coated silver nanoparticles. Sci. Total Environ. 454–455, 119–131.
Baalousha, M., Arkill, K.P., Romer, I., Palmer, R.E., Lead, J.R., 2015. Transformations of citrate and Tween coated silver nanoparticles reacted with Na2S. Sci. Total Environ. 502, 344–353.
Baalousha, M., Sikder, M., Prasad, A., Lead, J., Merrifield, R., Chandler, G.T., 2016. EN15142 the concentration-dependent behaviour of nanoparticles. Environ. Chem. 13 (1).
Badawy, A.M.E., Luxton, T.P., Silva, R.G., Scheckel, K.G., Suidan, M.T., Tolaymat, T.M., 2010. Impact of environmental conditions (pH, ionic strength, and electrolyte type) on the surface charge and aggregation of silver nanoparticles suspensions. Environ. Sci. Technol. 44 (4), 1260–1266.
Brewer, S.H., Glomm, W.R., Johnson, M.C., Knag, M.K., Franzen, S., 2005. Probing BSA binding to citrate-coated gold nanoparticles and surfaces. Langmuir 21 (20), 9303–9307.
El Badawy, A.M., Scheckel, K.G., Suidan, M., Tolaymat, T., 2012. The impact of stabilization mechanism on the aggregation kinetics of silver nanoparticles. Sci. Total Environ. 429, 325–331.
Fabrega, J., Luoma, S.N., Tyler, C.R., Galloway, T.S., Lead, J.R., 2011. Silver nanoparticles: behaviour and effects in the aquatic environment. Environ. Int. 37 (2), 517–531.
Filella, M., 2007. Colloidal properties of submicron particles in natural waters. IUPAC Series on Analytical and Physical Chemistry of Environmental Systems 10, p. 17.
Foldbjerg, R., Dang, D.A., Autrup, H., 2011. Cytotoxicity and genotoxicity of silver nanoparticles in the human lung cancer cell line, A549. Arch. Toxicol. 85 (7), 743–750.
Frens, G., 1972. Particle size and sol stability in metal colloids. Colloid Polym. Sci. 250 (7), 736–741.
Gondikas, A.P., Jang, E.K., Hsu-Kim, H., 2010. Influence of amino acids cysteine and serine on aggregation kinetics of zinc and mercury sulfide colloids. J. Colloid Interface Sci. 347 (2), 167–171.
Gondikas, A.P., Morris, A., Reinsch, B.C., Marinakos, S.M., Lowry, G.V., Hsu-Kim, H., 2012. Cysteine-induced modifications of zero-valent silver nanomaterials: implications for particle surface chemistry, aggregation, dissolution, and silver speciation. Environ. Sci. Technol. 46 (13), 7037–7045.
Grillo, R., Rosa, A.H., Fraceto, L.F., 2015. Engineered nanoparticles and organic matter: a review of the state-of-the-art. Chemosphere 119, 608–619.
Gu, B., Schmitt, J., Chen, Z., Liang, L., McCarthy, J.F., 1995. Adsorption and desorption of different organic matter fractions on iron oxide. Geochim. Cosmochim. Acta 59 (2), 219–229.
Gunsolus, I.L., Mousavi, M.P.S., Hussein, K., Bühlmann, P., Haynes, C.L., 2015. Effects of humic and fulvic acids on silver nanoparticle stability, dissolution, and toxicity. Environ. Sci. Technol. 49 (13), 8078–8086.
Guo, L., Macdonald, R.W., 2006. Source and transport of terrigenous organic matter in the upper Yukon River: evidence from isotope (δ13C, Δ14C, and δ15N) composition of dissolved, colloidal, and particulate phases. Glob. Biogeochem. Cycles 20 (2).
Guo, D., Zhu, L., Huang, Z., Zhou, H., Ge, Y., Ma, W., Wu, J., Zhang, X., Zhou, X., Zhang, Y., 2013. Anti-leukemia activity of PVP-coated silver nanoparticles via generation of reactive oxygen species and release of silver ions. Biomaterials 34 (32), 7884–7894.
Horovitz, O., Tomoaia, G., Mocanu, A., Yupsanis, T., Tomoaia-Cotisel, M., 2007. Protein binding to gold colloids. Gold Bull. 40 (3), 213–218.
Hotze, E.M., Phenrat, T., Lowry, G.V., 2010. Nanoparticle aggregation: challenges to understanding transport and reactivity in the environment. J. Environ. Qual. 39 (6), 1909–1924.
Huynh, K.A., Chen, K.L., 2011. Aggregation kinetics of citrate and polyvinylpyrrolidone coated silver nanoparticles in monovalent and divalent electrolyte solutions. Environ. Sci. Technol. 45 (13), 5564–5571.
Kawata, K., Osawa, M., Okabe, S., 2009. In vitro toxicity of silver nanoparticles at noncytotoxic doses to HepG2 human hepatoma cells. Environ. Sci. Technol. 43 (15), 6046–6051.
Levard, C., Hotze, E.M., Lowry, G.V., Brown Jr., G.E., 2012. Environmental transformations of silver nanoparticles: impact on stability and toxicity. Environ. Sci. Technol. 46 (13), 6900–6914.
Levard, C., Mitra, S., Yang, T., Jew, A.D., Badireddy, A.R., Lowry, G.V., Brown, G.E., 2013a. Effect of chloride on the dissolution rate of silver nanoparticles and toxicity to *E. coli*. Environ. Sci. Technol. 47 (11), 5738–5745.
Levard, C.m., Mitra, S., Yang, T., Jew, A.D., Badireddy, A.R., Lowry, G.V., Brown Jr., G.E., 2013b. Effect of chloride on the dissolution rate of silver nanoparticles and toxicity to *E. coli*. Environ. Sci. Technol. 47 (11), 5738–5745.
Li, X., Lenhart, J.J., Walker, H.W., 2010. Dissolution-accompanied aggregation kinetics of silver nanoparticles. Langmuir 26 (22), 16690–16698.
Li, X., Lenhart, J.J., Walker, H.W., 2012. Aggregation kinetics and dissolution of coated silver nanoparticles. Langmuir 28 (2), 1095–1104.
Li, X., Schirmer, K., Bernard, L., Sigg, L., Pillai, S., Behra, R., 2015. Silver nanoparticle toxicity and association with the alga *Euglena gracilis*. Environ. Sci.: Nano 2 (6), 594–602.
Liu, J.Y., Sonshine, D.A., Shervani, S., Hurt, R.H., 2011. Controlled release of biologically active silver from nanosilver surfaces. Abstr. Pap. Am. Chem. Soc. 241, 1.
Louie, S.M., Tilton, R.D., Lowry, G.V., 2013. Effects of molecular weight distribution and chemical properties of natural organic matter on gold nanoparticle aggregation. Environ. Sci. Technol. 47 (9), 4245–4254.
Louie, S.M., Spielman-Sun, E.R., Small, M.J., Tilton, R.D., Lowry, G.V., 2015. Correlation of the physicochemical properties of natural organic matter samples from different sources to their effects on gold nanoparticle aggregation in monovalent electrolyte. Environ. Sci. Technol. 49 (4), 2188–2198.
Loza, K., Diendorf, J., Sengstock, C., Ruiz-Gonzalez, L., Gonzalez-Calbet, J.M., Vallet-Regi, M., Koller, M., Epple, M., 2014. The dissolution and biological effects of silver nanoparticles in biological media. J. Mater. Chem. B 2 (12), 1634–1643.
Luo, M., Huang, Y., Zhu, M., Tang, Y.-n., Ren, T., Ren, J., Wang, H. and Li, F., 2016. Properties of different natural organic matter influence the adsorption and aggregation behavior of TiO_2 nanoparticles. J. Saudi Chem. Soc. https://doi.org/10.1016/j.jscs.2016.01.007.
Luoma, S.N., Stoiber, T., Croteau, M.-N., Römer, I., Merrifeld, R., Lead, J.R., 2016. Effect of cysteine and humic acids on bioavailability of Ag from Ag nanoparticles to a freshwater snail. NanoImpact 2, 61–69.
Mandal, S., Gole, A., Lala, N., Gonnade, R., Ganvir, V., Sastry, M., 2001. Studies on the reversible aggregation of cysteine-capped colloidal silver particles interconnected via hydrogen bonds. Langmuir 17 (20), 6262–6268.
Miao, A.-J., Schwehr, K.A., Xu, C., Zhang, S.-J., Luo, Z., Quigg, A., Santschi, P.H., 2009. The algal toxicity of silver engineered nanoparticles and detoxification by exopolymeric substances. Environ. Pollut. 157 (11), 3034–3041.
Mirshahghassemi, S., Lead, J.R., 2015. Oil recovery from water under environmentally relevant conditions using magnetic nanoparticles. Environ. Sci. Technol. 49 (19), 11729–11736.
Mirshahghassemi, S., Cai, B., Lead, J.R., 2016. Evaluation of polymer-coated magnetic nanoparticles for oil separation under environmentally relevant conditions: effect of ionic strength and natural organic macromolecules. Environ. Sci.: Nano 3, 780–787.
Mitra, C., Gummadidala, P.M., Afshinnia, K., Merrifield, R.C., Baalousha, M., Lead, J.R., Chanda, A., 2017. Citrate-coated silver nanoparticles growth-independently inhibit aflatoxin synthesis in aspergillus parasiticus. Environ. Sci. Technol. 51 (14), 8085–8093.
Moosa, A., Ridha, A., Allawi, M., 2015. Green Synthesis of Silver Nanoparticles Using Spent Tea Leaves Extract with Atomic Force Microscopy.
Moskovits, M., Vlckova, B., 2005. Adsorbate-induced silver nanoparticle aggregation kinetics. J. Phys. Chem. B 109 (31), 14755–14758.
Nebbioso, A., Piccolo, A., 2013. Molecular characterization of dissolved organic matter (DOM): a critical review. Anal. Bioanal. Chem. 405 (1), 109–124.
Paramelle, D., Sadovoy, A., Gorelik, S., Free, P., Hobley, J., Fernig, D.G., 2014. A rapid method to estimate the concentration of citrate capped silver nanoparticles from UV-visible light spectra. Analyst 139 (19), 4855–4861.
Peijnenburg, W.J.G.M., Baalousha, M., Chen, J., Chaudry, Q., Von der kammer, F., Kuhlbusch, T.A.J., Lead, J., Nickel, C., Quik, J.T.K., Renker, M., 2015. A review of the properties and processes determining the fate of engineered nanomaterials in the aquatic environment. Crit. Rev. Environ. Sci. Technol. 45 (19), 2084–2134.
Philippe, A., Schaumann, G.E., 2014. Interactions of dissolved organic matter with natural and engineered inorganic colloids: a review. Environ. Sci. Technol. 48 (16), 8946–8962.

Piccolo, A., 2001. The supramolecular structure of humic substances. Soil Sci. 166 (11), 810–832.
Poblete, H., Agarwal, A., Thomas, S.S., Bohne, C., Ravichandran, R., Phopase, J., Comer, J., Alarcon, E.I., 2016. New insights into peptide–silver nanoparticle interaction: deciphering the role of cysteine and lysine in the peptide sequence. Langmuir 32 (1), 265–273.
Pokhrel, L.R., Dubey, B., Scheuerman, P.R., 2013. Impacts of select organic ligands on the colloidal stability, dissolution dynamics, and toxicity of silver nanoparticles. Environ. Sci. Technol. 47 (22), 12877–12885.
Pokhrel, L.R., Andersen, C.P., Rygiewicz, P.T., Johnson, M.G., 2014. Preferential interaction of Na + over K + with carboxylate-functionalized silver nanoparticles. Sci. Total Environ. 490, 11–18.
Priester, J.H., Singhal, A., Wu, B., Stucky, G.D., Holden, P.A., 2014. Integrated approach to evaluating the toxicity of novel cysteine-capped silver nanoparticles to *Escherichia coli* and *Pseudomonas aeruginosa*. Analyst 139 (5), 954–963.
Ravindran, A., Dhas, S.P., Chandrasekaran, N., Mukherjee, A., 2013. Differential interaction of silver nanoparticles with cysteine. J. Exp. Nanosci. 8 (4), 589–595.
Romer, I., White, T.A., Baalousha, M., Chipman, K., Viant, M.R. and Lead, J.R. (2011) J Chromatogr A, pp. 4226–4233 , 2011 Elsevier B.V, Netherlands.
Samadi-Maybodi, A., Akhoondi, R., 2015. Trace analysis of N-acetyl-L-cysteine using luminol–H_2O_2 chemiluminescence system catalyzed by silver nanoparticles. Luminescence 30 (6), 775–779.
Sigg, L., Lindauer, U., 2015. Silver nanoparticle dissolution in the presence of ligands and of hydrogen peroxide. Environ. Pollut. 206, 582–587.
Stewart, A., Zheng, S., McCourt, M.R., Bell, S.E.J., 2012. Controlling assembly of mixed thiol monolayers on silver nanoparticles to tune their surface properties. ACS Nano 6 (5), 3718.
Thio, B.J.R., Zhou, D., Keller, A.A., 2011. Influence of natural organic matter on the aggregation and deposition of titanium dioxide nanoparticles. J. Hazard. Mater. 189 (1), 556–563.
Wijnhoven, S.W.P., Peijnenburg, W., Herberts, C.A., Hagens, W.I., Oomen, A.G., Heugens, E.H.W., Roszek, B., Bisschops, J., Gosens, I., Van de Meent, D., Dekkers, S., De Jong, W.H., Van Zijverden, M., Sips, A., Geertsma, R.E., 2009. Nano-silver - a review of available data and knowledge gaps in human and environmental risk assessment. Nanotoxicology 3 (2), 109–U178.
Yang, X., Lin, S., Wiesner, M.R., 2014a. Influence of natural organic matter on transport and retention of polymer coated silver nanoparticles in porous media. J. Hazard. Mater. 264, 161–168.
Yang, X., Lin, S., Wiesner, M.R., 2014b. Influence of natural organic matter on transport and retention of polymer coated silver nanoparticles in porous media. J. Hazard. Mater. 264 (Supplement C), 161–168.
Yi, F., Chen, G., Zeng, G., Guo, Z., Liu, W., Huang, Z., He, K., Hu, L., 2016. Influence of cysteine and bovine serum albumin on silver nanoparticle stability, dissolution, and toxicity to *Phanerochaete chrysosporium*. RSC Adv. 6 (108), 106177–106185.
Yin, Y., Shen, M., Tan, Z., Yu, S., Liu, J., Jiang, G., 2015. Particle coating-dependent interaction of molecular weight fractionated natural organic matter: impacts on the aggregation of silver nanoparticles. Environ. Sci. Technol. 49 (11), 6581–6589.
Zhang, W., Crittenden, J., Li, K., Chen, Y., 2012. Attachment efficiency of nanoparticle aggregation in aqueous dispersions: modeling and experimental validation. Environ. Sci. Technol. 46 (13), 7054–7062.